molecular pharmaceutics

Article

pubs.acs.org/molecularpharmaceutics

Intravenous Delivery of Hydrophobin-Functionalized Porous Silicon Nanoparticles: Stability, Plasma Protein Adsorption and Biodistribution

Mirkka Sarparanta,*[,†] Luis M. Bimbo,[‡] Jussi Rytkönen,[§] Ermei Mäkilä,[∥] Timo J. Laaksonen,[‡] Päivi Laaksonen,[⊥] Markus Nyman,[†] Jarno Salonen,[∥] Markus B. Linder,[⊥] Jouni Hirvonen,[‡] Hélder A. Santos,[‡] and Anu J. Airaksinen[†]

[†]Laboratory of Radiochemistry, Department of Chemistry and [‡]Division of Pharmaceutical Technology, Faculty of Pharmacy, FI-00014 University of Helsinki, Finland

[§]Department of Biosciences, University of Eastern Finland, FI-70211 Kuopio, Finland

[∥]Laboratory of Industrial Physics, Department of Physics and Astronomy, FI-20014 University of Turku, Finland

[⊥]Nanobiomaterials, VTT Technical Research Centre of Finland, FI-02044 VTT, Finland

Supporting Information

ABSTRACT: Rapid immune recognition and subsequent elimination from the circulation hampers the use of many nanomaterials as carriers to targeted drug delivery and controlled release in the intravenous route. Here, we report the effect of a functional self-assembled protein coating on the intravenous biodistribution of ^{18}F-labeled thermally hydrocarbonized porous silicon (THCPSi) nanoparticles in rats. ^{18}F-Radiolabeling enables the sensitive and easy quantification of nanoparticles in tissues using radiometric methods and allows imaging of the nanoparticle biodistribution with positron emission tomography. Coating with *Trichoderma reesei* HFBII altered the hydrophobicity of ^{18}F-THCPSi nanoparticles and resulted in a pronounced change in the degree of plasma protein adsorption to the nanoparticle surface *in vitro*. The HFBII-THCPSi nanoparticles were biocompatible in RAW 264.7 macrophages and HepG2 liver cells making their intravenous administration feasible. *In vivo*, the distribution of the nanoparticles between the liver and spleen, the major mononuclear phagocyte system organs in the body, was altered compared to that of uncoated ^{18}F-THCPSi. Identification of the adsorbed proteins revealed that certain opsonins and apolipoproteins are enriched in HFBII-functionalized nanoparticles, whereas the adsorption of abundant plasma components such as serum albumin and fibrinogen is decreased.

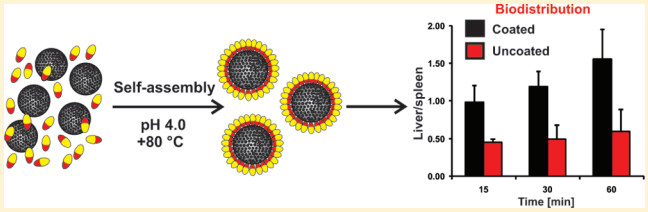

KEYWORDS: *porous silicon, hydrophobin, nanoparticle, protein adsorption, biodistribution*

1. INTRODUCTION

The demonstrated biocompatibility and versatile physicochemical properties of porous silicon (PSi) (e.g., particle size and shape, surface chemistry, pore size and degree of porosity) make it a promising material for carrier-mediated drug delivery.[1−3] PSi nano- and microparticles have been successfully used as carriers for poorly water-soluble drugs,[4−6] peptides,[7,8] siRNA,[9] and secondary nanoparticles,[10] yielding controlled and sustained release. *In vivo*, PSi is degraded to nontoxic silicic acid and the rate of biodegradation can be modified by the porosity and surface chemistry of the material.[11,12] However, like most foreign material in the body, PSi nanoparticles are often rapidly recognized and scavenged from the bloodstream by the cells of the mononuclear phagocyte system (MPS), which results in limited circulation time and accumulation to the spleen and liver, and thus hampers the efficient delivery of the payload to the target site after intravenous administration. Intravenously administered nanoparticles are eliminated from the circulation primarily by two cell populations: Kupffer cells in the liver and macrophages and B cells in the spleen.[13] The current understanding on nanoparticle biofate after its introduction to the bloodstream underlines the formation of a plasma-protein-derived corona on the nanoparticle surface.[14,15] The corona consists of plasma proteins that preferentially adsorb to the nanoparticle surface depending primarily on its wettability and surface charge density (ζ-potential). In general, plasma proteins are adsorbed more rapidly and in greater amounts to hydrophobic and/or charged particles.[16−18] Furthermore, the amount and identity of the adsorbed proteins does not necessarily replicate their relative abundances in plasma, as plasma proteins have different affinities for different surface properties or functionalization.[19] Certain plasma proteins, such as immunoglobulins, complement factors and some apolipo-

Received: November 30, 2011
Revised: January 13, 2012
Accepted: January 25, 2012
Published: January 25, 2012

proteins, are identified as opsonins, meaning that their adsorption will act as a signal for the macrophages of the MPS to engulf particles decorated with them. Others, like serum albumin, are considered to be so-called dysopsonins that can potentially prevent the opsonization process from occurring and possibly increase the circulation time of the nanoparticle.[16]

The main approaches to overcome the plasma protein adsorption include surface modification of the nanomaterial with polymers such as poly(ethylene glycol) (PEG) and dextran.[20,21] Covalent binding of known dysopsonins, such as BSA, has also been investigated.[22] However, the majority of these studies concern polymer and lipid nanoparticles for which hydrodynamic radii of 100 to 200 nm are easily achieved, further increasing the odds of prolonging their circulation time with the modification. Conversely, because of their top-down production methods, PSi nanoparticles are usually larger than 100 nm or even designed to be in the micrometer range to allow substantially higher loading capacities.[23,24] Dextran-coating and PEGylation of PSi nanoparticles has been reported in the literature, but the aim in these studies was to affect the rate of material biodegradation rather than increase the circulation time, and the latter remained largely undiscussed.[11,25]

In this study, thermally hydrocarbonized porous silicon (THCPSi) nanoparticles were biofunctionalized with a self-assembled protein coating consisting of a fungal protein, class II hydrophobin HFBII from *Trichoderma reesei*.[26,27] Hydrophobins are small amphiphilic proteins that have the interesting ability to sense the hydrophilicity/hydrophobicity of a surface and arrange to a monolayer that effectively alters the wettability of the material.[27] Hydrophobins have been used to improve the solubility of poorly water-soluble drug nanoparticles and construct drug delivery excipients with nanofibrillar cellulose.[28−31] We have previously shown that HFBII-functionalization does not affect the biocompatibility of THCPSi microparticles in cell models for oral drug delivery and that drug release is not impaired by the coating of drug-loaded particles with HFBII.[32] In addition, hydrophobins have been shown to influence secondary protein adsorption on surfaces, a phenomenon that could have use in the prevention of biofouling and design of biocompatible materials.[33,34] Interestingly, hydrophobins have even been reported to prevent the immune recognition of inhaled fungal spores,[35] but this property has not yet been studied for other HFBII-functionalized foreign particulates after systemic administration.

Here, we have investigated the stability of the HFBII coating on THCPSi nanoparticles in physiological conditions. The effect of the surface biofunctionalization on biocompatibility of the nanoparticles was studied *in vitro* in cell lines relevant to intravenous administration, namely, in RAW 264.7 macrophages and HepG2 hepatocellular carcinoma cells. HFBII-THCPSi nanoparticles radiolabeled with a short-lived positron emitter ^{18}F ($t_{1/2}$ = 109.8 min) were intravenously administered to rats to investigate the effect of the biofunctionalization on nanoparticle biodistribution *in vivo*. Plasma protein adsorption to the nanoparticles was studied *in vitro* in human plasma, and the most abundant adsorbed proteins were identified with proteomics.

2. MATERIALS AND METHODS

2.1. Synthesis of HFBII-Coated ^{18}F-THCPSi Nanoparticles. THCPSi nanoparticles were prepared as described previously from monocrystalline p+-type boron-doped Si(100) wafers anodized in hydrofluoric acid (38%)−ethanol (1:1, v/v) and treated with N_2:acetylene at +500 °C.[36,37] The nanoparticles were characterized with N_2 sorption measurement at 77 K (Tristar 3000, Micromeritics, Inc.), and results for the specific surface area and pore volume, diameter and porosity were calculated from the Brunauer−Emmett−Teller (BET) and Barrett−Joyner−Halenda (BJH) theories. The particles had specific surface area of 323 ± 3 m^2/g, pore volume of 0.48 ± 0.01 cm^3/g, pore diameter of 7.4 ± 0.2 nm and porosity of 53%. HFBII was produced and purified using established methods as described earlier. The HFBII-coating procedure was adapted to ^{18}F-radiolabeled nanoparticles from a method developed for PSi microparticles.[32]

^{18}F-Radiolabeling of THCPSi nanoparticles was carried out as described previously.[36,38] All reagents were purchased from Sigma-Aldrich and used without further purification. Briefly, ^{18}F from an ^{18}O(p,n)^{18}F irradiation on an IBA Cyclone 10/5 cyclotron was trapped in an anion exchange cartridge (Sep-Pak QMA Light Plus, Waters Corporation) and eluted as $^{18}F^-$/Kryptofix2.2.2/K^+ complex. After azeotropic distillation, 1.4−1.8 GBq of the dried complex was dissolved in anhydrous dimethylformamide with 4% (v/v) acetic acid. The solution was added to 1 mg of THCPSi nanoparticles suspended in 100 μL of DMF and heated for 10 min at +120 °C. Particles were separated from the reaction mixture with centrifugation at 15000*g* for 10 min and washed with 10 min sonications in 1 mL of absolute ethanol (Altia Corporation) followed by 1 mL of ultrapure water. The nanoparticles were collected with centrifugation between washes and resuspended carefully prior to sonication. Finally, the washed nanoparticles were resuspended in 100 μL of absolute ethanol.

In the coating procedure the ethanolic ^{18}F-THCPSi nanoparticle solution was slowly added to a solution of 4.0 ± 0.1 mg/mL of HFBII in McIlvaine buffer (pH = 4.0, 0.2 M Na_2HPO_4−0.1 M citrate). The solution was incubated for 30 min at +80 °C. Particles were separated from the coating solution with centrifugation and washed with 3 × 1 mL of ultrapure water. HFBII-^{18}F-THCPSi nanoparticles were formulated in sterile 0.9% NaCl to a final concentration of 107.2 ± 8.7 MBq/mL (1.48 ± 0.16 mg/mL). Specific radioactivity was determined from a 0.1 mL aliquot of the formulated solution washed with 3 × 1 mL of ultrapure water, freeze-dried overnight and weighed.

2.2. Characterization of HFBII-^{18}F-THCPSi Nanoparticles. For size and ζ-potential measurements, 0.1 mL samples were drawn from the formulated solution. In the ζ-potential samples, the particles were freed from NaCl by washing with 3 × 1 mL of ultrapure water and suspended in 1 mL of ultrapure water. For the size distribution measurements, particles were not washed and sample volume was only reconstituted to 1 mL with ultrapure water. Zeta potential was calculated from the electrophoretic mobility using the Smoluchowski relation. Size distribution from dynamic light scattering (DLS) and ζ-potential distribution were measured on a ZetaSizer Nano instrument (Malvern Ltd.).

HFBII content in the formulated particles was measured from the sample used for the determination of specific radioactivity. HFBII was dissolved from the particles by incubation in 2.5% (w/v) SDS−0.5% (v/v) ethanol at ambient temperature for 48 h. Particles were pelleted with centrifugation, and HFBII in the supernatant was quantified by a BCA (bicinchoninic acid) protein assay kit (Thermo Fisher Scientific) according to the manufacturer's instructions.

2.3. Synthesis of ^{125}I-Radiolabeled HFBII. HFBII was radiolabeled with ^{125}I in 10^{-5} M NaOH (pH 8−10, reductant-free, Perkin-Elmer Inc.) using standard procedure for radioiodination with the Bolton−Hunter method.[39] SHPP (*N*-succinimidyl-3-(hydroxyphenyl)propionate) was synthesized from 3-(4-hydrophenyl)propionic acid and *N*-hydrosuccinimide as described previously.[40] Purity of ^{125}I-SHPP was checked with thin layer chromatography (TLC) on a Merck Kieselgel 60 F_{254} plate developed with 9:1 (v/v) ethyl acetate−methanol. 50 μL of 1 mg/mL HFBII in 100 mM sodium borate buffer (pH = 8.5) was added to the dried ^{125}I-SHPP, and the reaction mixture was incubated at +40 °C for 45 min. ^{125}I-HFBII was purified on a PD MiniTrap G-25 column (GE Healthcare) preconditioned with 8 mL of McIlvaine buffer. The product was eluted with 3 mL of the buffer collecting 200 μL fractions. Fractions were measured on a dose calibrator (VDC-405, Veenstra Instruments) and peak fractions pooled. A 0.2 μL sample from the pooled peak fractions was spotted on Whatman 1 chromatography paper (Millipore Corporation) and developed with 50:50 (v/v) methanol−water for determination of radiochemical purity of ^{125}I-HFBII. The TLC plates and chromatography papers were subsequently exposed to a digital imaging plate (BAS SR2040, Fujifilm Corporation) for 48 h. The imaging plate was scanned on a Fujifilm FLA-5100 scanner, and the autoradiographs were analyzed with AIDA 2.0 imaging software (Raytest Isotopenmessgeräte GmbH). Immediately after pooling, 0.1 mg of HFBII carrier in McIlvaine buffer was added to the ^{125}I-HFBII solution to prevent adsorption to vial walls. HFBII in the final product was quantified against a standard series on a Shimadzu Prominence UFLC liquid chromatography system consisting of two LC-20AD pumps, SIL-20AHT autosampler, CTO-20AC column oven, SPD-20A UV/vis detector and an external NaI scintillation crystal radiodetector operated at +0.90 kV with an Agilent Zorbax Eclipse XDB-C_8 column (4.6 × 150 mm, 3.5 μm particle size) in 80:20 0.1% trifluoroacetic acid (TFA) in H_2O−0.08% TFA in acetonitrile at 2.5 mL/min, detection at 205 nm. A linear gradient of 0.08% TFA in acetonitrile to 60% was applied over 7 min.

2.4. Coating Stability. Coating of nonradioactive THCPSi nanoparticles with ^{125}I-HFBII was carried out analogously to the coating of the ^{18}F-labeled THCPSi for the biodistribution study, except that the coating solution was spiked with 0.2 MBq of ^{125}I-HFBII tracer in approximately 300 μL of McIlvaine buffer. Reaction volume was reconstituted to 1 mL with the buffer, and a 1:4 (w/w) ratio of nanoparticles to HFBII was maintained. The stability of the HFBII coating was investigated *in vitro* in 1× PBS, pH = 7.4 and in human plasma. Anonymous donor plasma was obtained from the Finnish Red Cross Blood Service (ethical permissions 55/2008 and 25/2011). Plasma incubations were carried out at +37 °C to stimulate enzymatic action. For the stability tests, freshly prepared ^{125}I-HFBII-coated particles were suspended in 100 μL of 1× PBS, pH = 7.4 and added to 5 mL of the buffer or plasma. At the designated time points (10, 30, 60, 120, and 240 min), 200 μL samples were drawn from the incubation and particles were pelleted by centrifugation. Radioactivity of the particle pellets and supernatants was counted in an automated gamma counter (Wizard 3, Perkin-Elmer) for 5 min. In order to identify the radioactive species (i.e., free $^{125}I^-$ vs ^{125}I-HFBII), a 1 μL sample from all supernatants was spotted on Whatman 1 chromatography paper (Millipore Corporation) and processed and analyzed with digital autoradiography as described above. All stability tests were performed in duplicate on two different batches of ^{125}I-HFBII-THCPSi.

2.5. Cell Culture and Viability Assays. The *in vitro* studies with the coated and uncoated THCPSi nanoparticles were done on a human liver hepatocellular carcinoma, HepG2, and a murine leukemic monocyte macrophage cell line, RAW 264.7 (American Type Culture Collection, USA). The HepG2 cells were cultured in 75 cm^2 culture flasks (Corning Life Sciences Inc.) using Dulbecco's modified Eagle's medium (DMEM, EuroClone S.p.A., Italy) with 4.5 g/L glucose and 1% sodium pyruvate, supplemented with 10% fetal bovine serum (FBS, Gibco, Invitrogen), 1% nonessential amino acids, 1% L-glutamine, penicillin (100 IU/mL), and streptomycin (100 mg/mL) (all from EuroClone S.p.A.). RAW 264.7 macrophages were cultured in similar conditions as the HepG2, but without sodium pyruvate. The cultures were maintained in a BB 16 gas incubator at +37 °C (Heraeus Instruments GmbH) in an atmosphere of 5% CO_2 and 95% relative humidity. The growth medium was changed every other day. The HepG2 from passages 20−24 and RAW 264.7 macrophage cells from passages 10−17 were used in the experiments. Prior to each test, the cells were harvested using 0.25% (v/v) trypsin−ethylenediamine tetraacetic acid (EDTA)−phosphate buffer solution. For the cell viability assessment, 100 μL of a 5 × 10^5 cells/mL of HepG2 and 2.5 × 10^5 cells/mL of RAW 264.7 macrophage solution in DMEM were seeded in 96-well plates (PerkinElmer Inc.) and allowed to attach overnight. The medium was aspirated and the wells washed twice with fresh 1× HBSS (Hanks balanced salt solution). Subsequently, 100 μL of uncoated and HFBII-coated THCPSi nanoparticle suspensions with concentrations of 250, 100, 50, and 15 μg/mL were added to the wells. Incubations with 1× HBSS and Triton X-100 were used as positive and negative controls, respectively. After 3 and 12 h of incubation, the wells were washed once with 1× HBSS and the number of viable cells was assayed with CellTiter-Glo (Promega Corporation) according to the manufacturer's instructions. The luminescence was measured on a Varioskan Flash fluorometer (Thermo Fisher Scientific). All the assays were carried out at least in quadruplicate.

2.6. *In Vitro* Plasma Protein Adsorption. In order to determine the influence of HFBII coating on the secondary adsorption of plasma proteins to THCPSi nanoparticles, uncoated THCPSi and coated HFBII-THCPSi nanoparticles (90 μg each) were suspended in 1 mL of human plasma in 1.5 mL polypropylene centrifuge tubes (Protein LoBind, Eppendorf GmbH). The samples were incubated at +37 °C for 15, 60, and 120 min. After the incubations the particles were collected with centrifugation and washed twice with 1 mL of ultrapure water. The particles were resuspended in 1 mL of ultrapure water and their particle size and ζ-potential measured as described earlier. Size distribution peak analysis was performed with multiple Gaussian peak fit and integration in Origin (version 7.5, OriginLab Corporation).

2.7. Biodistribution Studies. All experimental procedures were approved by the National Board for Animal Experimentation in Finland (State Provincial Office of Southern Finland, Hämeenlinna) and conducted in accordance with the European Commission directive 2010/63/EU. Male Wistar:-Han rats (226−378 g, 8−14 weeks, Harlan, Horst, The Netherlands) were used in the biodistribution study. Animals were group-housed in standard polycarbonate cages with aspen bedding with food (Harlan Teklad Global Diet 2018) and tap water available ad libitum. Environmental conditions of a 12:12

lighting rhythm, temperature of 22 ± 1 °C, and relative humidity of 60 ± 5% were maintained throughout the study. Animals were single-housed and fasted for 18 h before dosing. 15.8 ± 3.3 MBq of HFBII-^{18}F-THCPSi nanoparticles in sterile 0.9% NaCl were administered intravenously to the lateral tail vein via a temporary 24-gauge catheter under 1.5−2.5% isoflurane (IsoFlo Vet, Orion Pharma, Espoo, Finland) anesthesia in O_2 carrier at 2.5 L/min. Control rats received 4.1 ± 1.4 MBq of ^{18}F-NaF in sterile 0.9% NaCl to assess the biodistribution of free $^{18}F^-$ in the experimental setup and determine the *in vivo* stability of the label in HFBII-^{18}F-THCPSi. A third group of animals received uncoated ^{18}F-THCPSi nanoparticles in 5% Solutol−1× HBSS (pH = 7.4) to supplement data acquired earlier.[36] Animals (n = 3−4 per time point) were sacrificed at 15, 30, and 60 min after administration with CO_2 asphyxiation followed by cervical dislocation. Samples from blood, urine and major organs were collected, weighed and counted in an automated gamma counter (Wizard 3, Perkin-Elmer) for 60 s.

2.8. Identification of Adsorbed Plasma Proteins. Identification of adsorbed plasma proteins was carried out from nanoparticle samples (section2.6) incubated in human plasma for 120 min at +37 °C. The proteins were extracted from the nanoparticles with 15 μL of SDS−PAGE sample buffer (125 mM Tris-HCl pH 6.8, 2% SDS, 5% glycerol, 0.002% bromophenol blue) and incubated at +100 °C for 5 min in order to release and denaturate the adsorbed proteins. The samples were run on a 9% SDS−PAGE gel for 2.5 h at with a constant voltage of 100 V. The gel was stained with 0.025% Coomassie brilliant blue (Thermo Fisher Scientific). Major protein bands were excised and digested in-gel using sequencing grade modified trypsin (Promega Corporation) at +37 °C, pH 8 for 16 h.

The tryptic digests were separated with liquid chromatography and analyzed with a QSTAR XL hybrid quadrupole time-of-flight mass spectrometer (Applied Biosystems). The proteins were identified from peptide mass fingerprint data with MASCOT search engine (v1.6b25 script 27, http://www.matrixscience.com). The used hardware and HPLC methods will be described in detail elsewhere (Rytkönen et al., 2011, submitted). The mass spectrometer was calibrated with known trypsin autolytic peptides. The MASCOT searches were carried out against the UniProt database (release 2011_09, http://www.uniprot.org/) that contained 532 146 sequences. Parent ion and fragment mass tolerances were 0.1 and 0.2 Da, respectively. Oxidation of methionine (M) was selected as a variable modification.

2.9. Statistical Analysis. Statistical analysis of the results was carried out with Student's t-test on PASW Statistics (version 18.0.0, IBM Corporation) or GraphPad Prism software (version 5.01, GraphPad Software). P values of <0.05 between THCPSi and HFBII-THCPSi were considered statistically significant.

3. RESULTS AND DISCUSSION

3.1. Synthesis of HFBII-^{18}F-THCPSi Nanoparticles. Freshly labeled ^{18}F-THCPSi nanoparticles were successfully coated with HFBII in a one-step procedure. Product specific radioactivity was 73.4 ± 13.9 MBq/mg (107.2 ± 8.7 MBq/mL, particle concentration 1.48 ± 0.16 mg/mL) at the end of synthesis. Total synthesis time from the end of bombardment for ^{18}F production to the end of synthesis was 185 ± 13 min, which is satisfactory with respect to the half-life of the isotope without compromise to end product yield. The overall decay-corrected radiochemical yield for HFBII-^{18}F-THCPSi was 40.2 ± 5.3%. A marked change in the behavior of the particles in solution was induced by the coating as coated particles dispersed easily to 0.9% NaCl and remained in solution, whereas uncoated, hydrophobic THCPSi tended to aggregate and sediment or float in the solution (Figure S1 in the Supporting Information). As a result, HFBII-^{18}F-THCPSi could be formulated into ultrapure water or aqueous solutions with physiological salt concentrations (e.g., saline, 1× HBSS, 1× PBS) without problems and subsequently evaluated in the biological models used in this study.

3.2. Nanoparticle Characterization. The HFBII content of the HFBII-^{18}F-THCPSi nanoparticles was determined to be 8.0 ± 0.5 wt % in the BCA assay. The average size of uncoated ^{18}F-THCPSi nanoparticles was 215 ± 54 nm and the average ζ-potential −33.70 ± 5.22 mV. The average size of HFBII-^{18}F-THCPSi nanoparticles in the formulated batches was 324 ± 53 nm and the average ζ-potential −26.70 ± 5.45 mV. The lack of pronounced change in the ζ-potential of the nanoparticles after the modification with HFBII suggests that the near-neutral charge of HFBII (pI 4.8) at pH 5.5 which renders the protein a relatively low charge density might not be sufficient to mask the negative charge of the underlying PSi surface.[41]

3.3. Coating Stability in Physiological Conditions. The stability of the HFBII coating on THCPSi nanoparticles was investigated *in vitro* in physiological conditions relevant for systemic administration. Coating stability curves are given in Figure 1. The coating was stable in 1× PBS (pH = 7.4), with

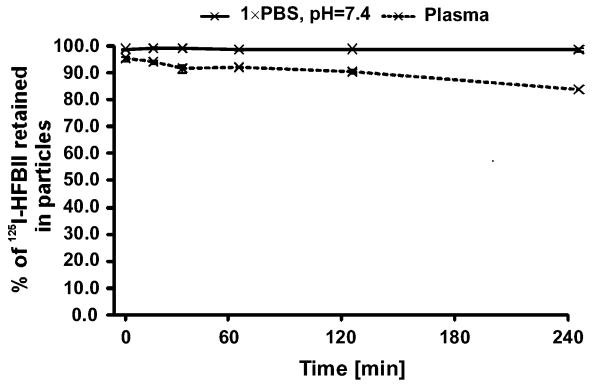

Figure 1. Stability of the HFBII coating on THCPSi nanoparticles in 1× PBS (pH = 7.4) and in human plasma at +37 °C. Values denote the average ± SD of two experiments.

98.7% of the ^{125}I-HFBII bound to the nanoparticles still after 240 min. In plasma, a gradual but minute loss of the coating was seen over time (83.8% particle-bound at 240 min). Paper chromatography of the supernatants from the stability tests (data not shown) confirmed that the loss of radioactivity from the particles in both cases was due to the detachment of intact ^{125}I-HFBII. Together these results indicate that circulating HFBII-^{18}F-THCPSi nanoparticles would retain their HFBII coating for hours after systemic administration, making the concept of prolonging circulation time with the biofunctionalization feasible. The ^{18}F-label itself on THCPSi has been shown to be stable in human plasma at +37 °C for 6 h.[38]

3.4. Cell Viability. The biocompatibility of the HFBII-THCPSi nanoparticles was studied in two cell lines relevant to parenteral administration. In RAW 264.7 macrophages (Figure

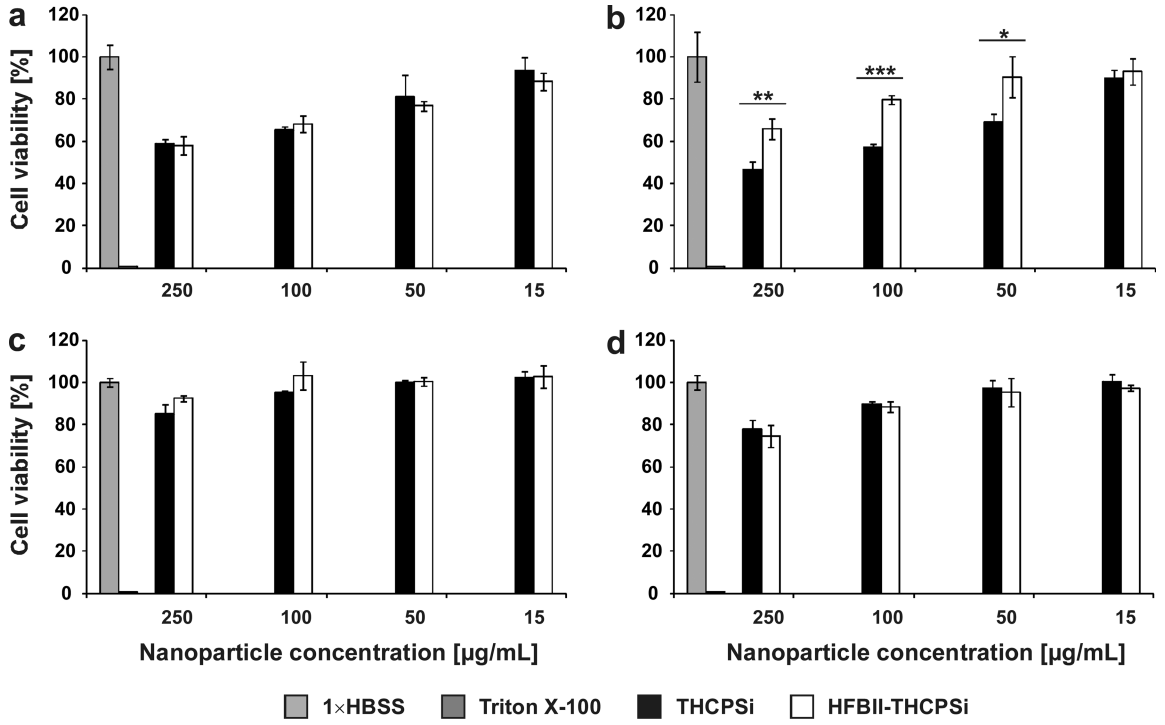

Figure 2. Cell viability in RAW 264.7 macrophages and HepG2 hepatocytes incubated with THCPSi and HFBII-THCPSi nanoparticles. RAW 264.7 at 3 and 12 h, respectively (a, b). HepG2 at 3 and 12 h, respectively (c, d). Columns denote average ± SD ($n \geq 4$). *$p \leq 0.05$, **$p \leq 0.01$, ***$p \leq 0.001$.

2a,b), significant increase in cell viability compared to uncoated THCPSi was observed for the three highest nanoparticle concentrations (50, 100, and 250 μg/mL) after 12 h for HFBII-THCPSi nanoparticles compared to their uncoated counterparts. However, similar effects were not seen either for the macrophages at 3 h or for the HepG2 hepatocytes at any time point (Figure 2c,d). Macrophages have previously been shown to be more sensitive to the cytotoxic effects of PSi particles, and possibly therefore the observed effect in increased biocompatibility was limited to this cell type.[5] Because of their hydrophobicity, THCPSi particles are inherently slightly more toxic than other types of surface-modified PSi, as they can potentially form strong cell−nanoparticle interactions leading to reduced cell viability.[42] In contrast, interactions of hydrophilic nanoparticles with cells could be mediated by weaker hydrophilic interactions between the nanoparticle surface, water molecules, and proteins of the cell membrane. The concentration of the most pronounced effects to the highest nanoparticle concentrations is in agreement with previous observations for PSi and non-PSi nanoparticles.[43] Based on these results, the *in vivo* biocompatibility of HFBII-THCPSi nanoparticles was expected to be comparable to or greater than that of uncoated THCPSi and their intravenous delivery was not contraindicated.

3.5. Effects of Plasma Protein Adsorption on the Size and ζ-Potential of HFBII-THCPSi and THCPSi Nanoparticles. In order to investigate the ability of the HFBII coating to alter the plasma protein adsorption on THCPSi nanoparticles, both coated and uncoated nanoparticles were incubated in human plasma at +37 °C. Rapid aggregation of THCPSi nanoparticles in plasma to aggregates that could not be broken down by extensive sonication (Figure 3a) was seen, whereas no aggregation was observed in the HFBII-coated nanoparticles (Figure 3b), illustrating that plasma protein adsorption is likely affected by the coating. Further analysis of the size distribution curves revealed that the average diameter of the THCPSi nanoparticle aggregates increased from 1 μm to almost 2 μm between 15 and 120 min of plasma incubation (Figure 3c). The fraction of nonaggregated nanoparticles determined from the size distribution measurements in the THCPSi incubations declined from 16.9% to 1.1% between 15 and 120 min. The ζ-potential of THCPSi nanoparticles rose to −9 mV (Figure 3d) after incubation in plasma. This is in line with a previous study, where incubation of negatively charged PSi with serum renders the surface charge near neutral.[44] On the contrary, only a minute increase from −21 to −17 mV in the ζ-potential was seen for the HFBII-THCPSi nanoparticles (Figure 3d), alluding to lesser extent of plasma protein adsorption in this particle type.

3.6. Biodistribution of HFBII-^{18}F-THCPSi Nanoparticles after Intravenous Administration and *in Vivo* Stability. The biodistribution data for HFBII-^{18}F-THCPSi nanoparticles after intravenous administration in rats is given in Table 1. Results are expressed as percentage of injected dose per gram of tissue (ID%/g). The highest uptake of the nanoparticles was seen in the liver and spleen, the major MPS organs. Interestingly, however, the HFBII coating significantly alters the liver-to-spleen ratio of ^{18}F-THCPSi uptake with roughly equal amounts of nanoparticles being distributed to the spleen and liver in HFBII-^{18}F-THCPSi-dosed animals, in contrast to the previous study with ^{18}F-THCPSi nanoparticles where the spleen uptake remained 2-fold to the liver uptake.[36] In addition, despite their larger size, lung uptake of HFBII-^{18}F-THCPSi was significantly lower than that of ^{18}F-THCPSi at 15 min, potentially reflecting the possibility that THCPSi nanoparticles could aggregate to a degree also *in vivo* resulting in entrapment into the lung capillary bed. When evaluated against the biodistribution of free $^{18}F^-$ label that favorably accumulates to

dx.doi.org/10.1021/mp200611d | *Mol. Pharmaceutics* 2012, 9, 654−663

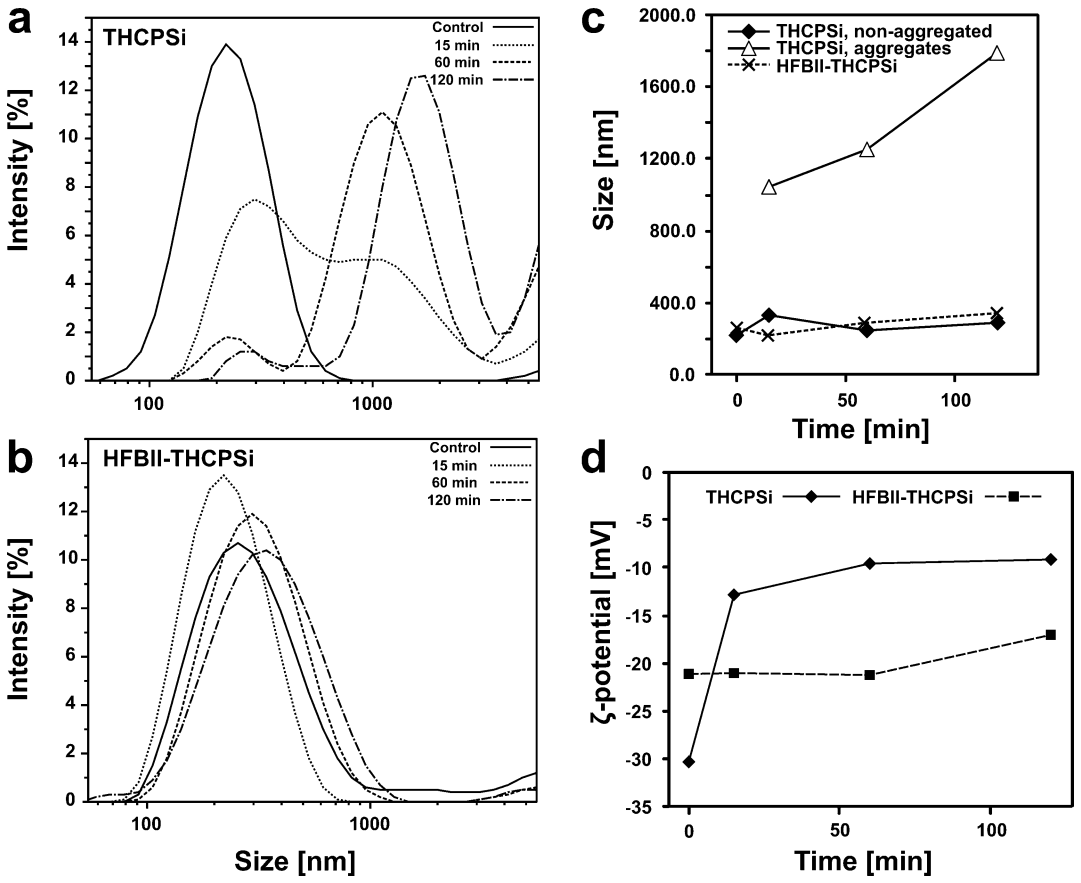

Figure 3. Effects of plasma protein adsorption on the size and ζ-potential of THCPSi and HFBII-THCPSi nanoparticles. (a) Size distributions for THCPSi from 15 to 120 min. (b) Size distributions for HFBII-THCPSi from 15 to 120 min. (c) Average size in nonaggregated and aggregated nanoparticle fractions for THCPSi and HFBII-THCPSi calculated from the DLS measurement data as a function of time. (d) ζ-potential for THCPSi and HFBII-THCPSi as a function of time.

Table 1. Biodistribution of HFBII-^{18}F-THCPSi and ^{18}F-THCPSi Nanoparticles in Rats after Intravenous Administration[a]

	HFBII-^{18}F-THCPSi (ID%/g)			^{18}F-THCPSi (ID%/g)		
	15 min	30 min	60 min	15 min	30 min	60 min
blood	0.02 ± 0.00	0.03 ± 0.02	0.01 ± 0.01	0.32 ± 0.15	0.45 ± 0.35	0.09 ± 0.05
GALT	0.01 ± 0.00	0.01 ± 0.00	0.02 ± 0.00	0.02 ± 0.01	0.04 ± 0.00	0.04 ± 0.01
stomach	0.02 ± 0.02	0.01 ± 0.00	0.01 ± 0.00	0.03 ± 0.02	0.12 ± 0.11	0.05 ± 0.05
liver	7.06 ± 1.27*	10.43 ± 2.98	9.07 ± 3.78	3.90 ± 0.79	6.34 ± 0.83	7.67 ± 1.46
lung	0.42 ± 0.11*	0.70 ± 0.32	0.55 ± 0.42	2.30 ± 1.58	0.73 ± 0.10	0.40 ± 0.14
kidney	0.05 ± 0.01	0.05 ± 0.03	0.03 ± 0.02	0.21 ± 0.06	0.35 ± 0.17	0.15 ± 0.08
spleen	7.28 ± 1.31	8.65 ± 1.70	6.22 ± 3.62	8.61 ± 1.36	14.35 ± 6.21	14.53 ± 5.21
testis	0.00 ± 0.00	0.00 ± 0.00	0.00 ± 0.00	0.01 ± 0.00	0.01 ± 0.00	0.01 ± 0.00
brain	0.00 ± 0.00	0.01 ± 0.00	0.00 ± 0.00	0.02 ± 0.01	0.03 ± 0.02	0.01 ± 0.01
bone	0.02 ± 0.00*	0.04 ± 0.01*	0.04 ± 0.02*	0.07 ± 0.01	0.15 ± 0.03	0.21 ± 0.05
heart	0.02 ± 0.01	0.04 ± 0.01	0.01 ± 0.00	0.47 ± 0.31	0.52 ± 0.52	0.76 ± 1.29
urine	0.15 ± 0.10	0.21 ± 0.29	0.40 ± 0.47	0.28 ± 0.13	0.55 ± 0.46	0.73 ± 0.44
liver/spleen	0.99 ± 0.22*	1.20 ± 0.20*	1.56 ± 0.39*	0.45 ± 0.05	0.49 ± 0.19	0.60 ± 0.29

[a]Values are the average ± SD for 3 or 4 animals, *$p \leq 0.05$. GALT: gut-associated lymphoid tissue.

the bone and is excreted via the kidneys[45] (depicted in Figure S2 in the Supporting Information), HFBII-^{18}F-THCPSi displayed an entirely different distribution pattern, demonstrating that the stability of the ^{18}F radiolabel is not adversely affected by the coating procedure and corroborating the finding that the uptake of radioactivity to the MPS organs is due to the uptake of the nanoparticles. In addition, significantly less $^{18}F^-$ is released and accumulates to bone from HFBII-coated particles compared to the uncoated ^{18}F-THCPSi, illustrating a protective effect of the coating on the underlying Si−^{18}F bond from hydrolytic cleavage *in vivo*.

3.7. Identification of Adsorbed Plasma Proteins *in Vitro*. The perplexing results of the biodistribution study led us to further investigate the composition of the plasma protein corona on the two nanoparticle types in order to explain the differences in their sequestration after intravenous delivery. Identification of the adsorbed plasma proteins was carried out with SDS−PAGE gel electrophoresis (Figure 4) followed by gel

dx.doi.org/10.1021/mp200611d | *Mol. Pharmaceutics* 2012, 9, 654−663

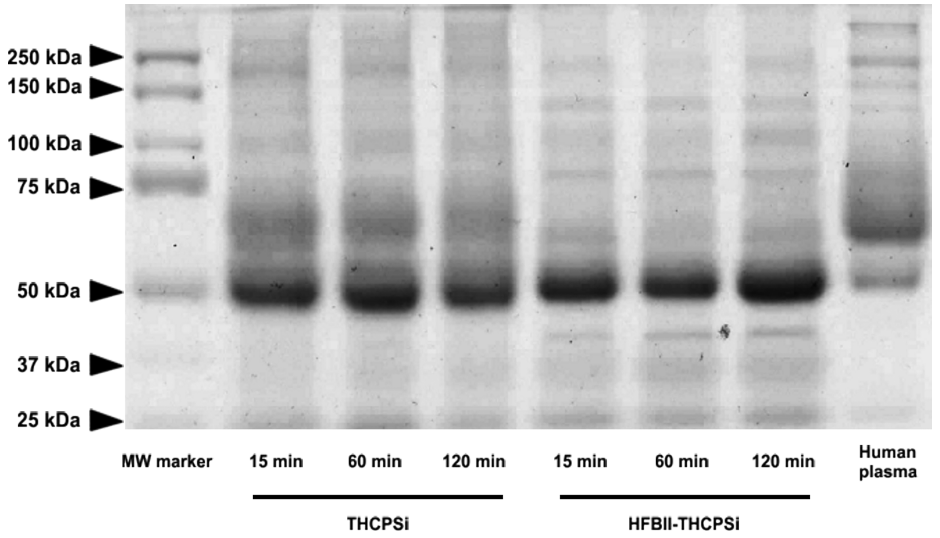

Figure 4. SDS–PAGE separation of the adsorbed plasma proteins in THCPSi and HFBII-THCPSi nanoparticles.

extraction, LC–MS analysis of the digests and proteomics search. The identified plasma proteins adsorbed to each nanoparticle type are summarized in Table 2. The analyzed bands on the gel and the MASCOT scores for all the identified proteins are given in Figure S3 and Table S1 in the Supporting Information, respectively. Out of the identified proteins, only inter-α-trypsin inhibitor heavy chain H4, immunoglobulin G (IgG, γ-1 and γ-2 chain C regions), and apolipoprotein A-I were found in both THCPSi and HFBII-THCPSi. A total of 9 proteins were detected for each particle type, but the identity of these proteins varied depending on the surface functionalization. All of the identified proteins are common hits in studies of protein adsorption to nanoparticles.[16−19] Curiously, abundant plasma components fibrinogen, serotransferrin, and serum albumin (HSA) were found only in THCPSi nanoparticles, whereas complement C3, IgM, apolipoproteins E and A-IV, and clusterin (apolipoprotein J) were found only in HFBII-THCPSi. Some proteins detected in the control plasma (α-2-macroglobulin, hemopexin, apolipoprotein B-100) were not detected in either nanoparticle sample. With the exception of IgG and fibrinogen, all the identified proteins have pI values that render them a negative or near neutral charge at physiological pH. Earlier studies with polystyrene nanoparticles bearing either positive or negative charge on their surface have implicated that particles with a negative ζ-potential bind proteins that have pI > 5.5.[18] Our results corroborate those of a recent report on protein adsorption to negatively charged silica nanoparticles, where a similar trend of adsorption of proteins with pI values less than 7 was seen.[19] In the work, Tenzer and co-workers postulate that this effect could be explained by the transient binding of positively charged plasma proteins to the nanoparticle surface that would then attract the negatively charged proteins, resulting in the observed final composition of the corona. Investigations on the kinetics of the plasma protein corona formation have suggested that the adsorption is often initiated by the abundant, but low-affinity plasma proteins (e.g., serum albumin, fibrinogen), followed by displacement with higher-affinity, less abundant proteins yielding the final corona over time.[46,47] Interestingly, we found both HSA and fibrinogen in THCPSi still after 120 min, whereas they could have been initially present and then replaced by the apolipoproteins E, A-IV and J in the HFBII-THCPSi nanoparticles. The presence of HSA and fibrinogen in THCPSi nanoparticles can probably be explained by the inclusion of the proteins to the nanoparticle aggregates formed already after 15 min of incubation. As fibrinogen is part of the blood coagulation cascade, it is possible that the observed aggregation was promoted by its adsorption to THCPSi nanoparticle surface. Several studies on nanomaterial biocompatibility have alluded to the possibility that the adsorbed plasma proteins would govern the biodistribution of nanoparticles to MPS organs, but a systematic evaluation of the contributions of individual opsonins to the sequestration between the liver and spleen is still lacking. IgG is known to stimulate phagocytosis of foreign particles to macrophages via a Fcγ-receptor mediated mechanism.[48] As IgG was found on both THCPSi and HFBII-THCPSi nanoparticles, the differ-

Table 2. Adsorbed Proteins Identified from THCPSi and HFBII-THCPSi Nanoparticles after 120 min of Incubation in 100% Human Plasma.

protein	nominal MW	pI[a]	THCPSi[a]	HFBII-THCPSi[a]
apolipoprotein B-100	515283	6.57	−	−
complement C3	187030	6.02	−	+
α-2-macroglobulin	163188	6.03	−	−
inter-α-trypsin inhibitor heavy chain H4	103293	6.51	+	+
fibrinogen α chain	94914	5.70	+	−
serotransferrin	77014	6.81	+	−
serum albumin	69321	5.92	+	−
fibrinogen β chain	55892	8.54	+	−
clusterin (apolipoprotein J)	52641	5.89	−	+
hemopexin	51643	6.55	−	−
fibrinogen γ chain	51479	5.37	+	−
IgM μ chain C region	49276	6.35	−	+
apolipoprotein A-IV	45371	5.28	−	+
apolipoprotein E	36132	5.65	−	+
IgG γ-1 chain C region	36083	8.46	+	+
IgG γ-2 chain C region	35878	7.66	+	+
apolipoprotein A-I	30759	5.56	+	+

[a]Isoelectric points calculated from the complete sequence retrieved from UniProt database using the built-in pI/MW calculator. [a](+) detected, (−) not detected.

dx.doi.org/10.1021/mp200611d | *Mol. Pharmaceutics* 2012, 9, 654–663

ences in their liver and spleen uptake cannot be solely accounted for by immunoglobulin-mediated uptake. Instead, the observed size increase of ^{18}F-THCPSi as a result of plasma protein adsorption could potentially contribute to increased splenic filtration and concentration of the particles to the spleen, as the splenic interendothelial cell slits ranging from 200 to 500 nm in diameter in humans and rats efficiently filter out foreign particulates that are too large or rigid to pass through them.[49] Smaller HFBII-^{18}F-THCPSi could, in contrast, escape similar physical removal in the spleen. However, further investigations on the nanoparticle size distribution *in situ* in plasma are needed in order to corroborate this. Proteins associated with immune recognition and phagocytosis dominate on the HFBII-THCPSi surface whereas serum albumin, a known dysopsonin, was not detected. IgM is known to promote complement activation and opsonization while complement factor C3 induces phagocytosis into Kupffer cells.[49,50] Apolipoproteins E and J in turn have been shown to promote recruitment of "non-professional" phagocytes, such as hepatocytes and cells of fibroblast origin, to the clearance of liposomes and cellular debris via lipoprotein receptor-mediated phagocytosis.[51,52] Therefore, phagocytic mechanisms could contribute to the removal of HFBII-^{18}F-THCPSi from the circulation and observed increase in the liver uptake versus accumulation to the spleen, but further studies are needed in order to demonstrate the presence of such mechanisms. Splenic filtration and uptake to resident macrophages in the spleen continue to play a role, but their contribution is decreased as a larger portion of the nanoparticles sequestrates to the liver.

However, rapid clearance from the circulation cannot be seen as solely a negative feature for a drug nanocarrier, as tailored recruitment of opsonins and subsequent uptake into a specific cell type (e.g., endothelial cells in vasculature or hepatocytes) may serve as means for targeted drug delivery.[24] Furthermore, nanoparticles and crystals that escape recognition by the MPS may produce adverse effects due to their limited or slow degradation and hindered elimination.[53] As the HFBII coating was shown to slowly leach out of the HFBII-THCPSi nanoparticles in plasma, it is very likely to be completely removed over time *in vivo* and therefore not likely to interfere with the biodegradation of the naked PSi particle, restoring one of the most acclaimed features of the nanomaterial.

4. CONCLUSION

Nanoparticle surface chemistry, charge and hydrophobicity are vital determinants for the formation of a plasma protein corona and subsequent MPS recognition of nanoparticles after intravenous delivery, although these features are not always immediately "visible" for the cells within the body. In this work, we have successfully addressed all these aspects for THCPSi nanoparticles modified with a self-assembled coating consisting of fungal hydrophobin. The biofunctionalization with HFBII was shown to modify the plasma protein adsorption to THCPSi nanoparticles, resulting in significant alteration in their accumulation to the liver and spleen. In conclusion, the observed coating-induced changes on HFBII-^{18}F-THCPSi nanoparticle biodistribution and plasma protein adsorption warrant further immunological profiling of HFBII-functionalized PSi nanoparticles and encourage studies on PSi particles modified with engineered variants of the protein for targeted drug delivery in the intravenous route.

■ ASSOCIATED CONTENT

Supporting Information

Photograph of the nanoparticle formulations, analyzed bands from SDS−PAGE, MASCOT scores for the identified adsorbed plasma proteins, and the biodistribution of HFBII-^{18}F-THCPSi nanoparticles compared to free $^{18}F^-$ in rats after intravenous administration. This material is available free of charge via the Internet at http://pubs.acs.org.

■ AUTHOR INFORMATION

Corresponding Author

*Laboratory of Radiochemistry, Department of Chemistry, P.O. Box 55, FI-00014 University of Helsinki, Finland. Tel: +358-9-191 50134. Fax: +358-9-191 50121. E-mail: mirkka.sarparanta@helsinki.fi.

Notes

The authors declare no competing financial interest.

■ ACKNOWLEDGMENTS

We thank Mrs. Helena Jauho for assistance with the size and zeta potential measurements. M.Sc. Janne Weisell (University of Eastern Finland, Kuopio) is acknowledged for skillful technical assistance with mass spectrometry. The HepG2 cells were a generous gift from Dr. Yan-Ru Lou (Division of Biopharmaceutics and Pharmacokinetics, University of Helsinki). Financial support from the Academy of Finland (Decision Numbers 127099, 123037, 122314, 136805, 127138 and 140965), the University of Helsinki Research Funds (Project Number 490039), the Jenny and Antti Wihuri Foundation, and the Drug Discovery Graduate School is gratefully acknowledged.

■ REFERENCES

(1) Salonen, J.; Kaukonen, A. M.; Hirvonen, J.; Lehto, V. Mesoporous Silicon in Drug Delivery Applications. *J. Pharm. Sci.* **2008**, *97*, 632−653.

(2) Anglin, E. J.; Cheng, L.; Freeman, W. R. Sailor, M.J. Porous Silicon in Drug Delivery Devices and Materials. *Adv. Drug Delivery Rev.* **2008**, *60*, 1266−1277.

(3) Prestidge, C. A.; Barnes, T. J.; Lau, C.; Barnett, C.; Loni, A.; Canham, L. Mesoporous Silicon: a Platform for the Delivery of Therapeutics. *Expert Opin. Drug Delivery* **2007**, *4*, 101−110.

(4) Wang, F.; Hui, H.; Barnes, T. J.; Barnett, C.; Prestidge, C. A. Oxidized Mesoporous Silicon Microparticles for Improved Oral Delivery of Poorly Soluble Drugs. *Mol. Pharmaceutics* **2010**, *7*, 227−236.

(5) Bimbo, L. M.; Mäkilä, E.; Laaksonen, T.; Lehto, V.; Salonen, J.; Hirvonen, J.; Santos, H. A. Drug Permeation Across Intestinal Epithelial Cells Using Porous Silicon Nanoparticles. *Biomaterials* **2011**, *32*, 2625−2633.

(6) Salonen, J.; Laitinen, L.; Kaukonen, A. M.; Tuura, J.; Björkqvist, M.; Heikkilä, T.; Vähä-Heikkilä, K.; Hirvonen, J.; Lehto, V.-P. Mesoporous Silicon Microparticles for Oral Drug Delivery: Loading and Release of Five Model Drugs. *J. Controlled Release* **2005**, *108*, 362−374.

(7) Kilpeläinen, M.; Riikonen, J.; Vlasova, M. A.; Huotari, A.; Lehto, V. P.; Salonen, J.; Herzig, K. H.; Järvinen, K. In vivo Delivery of a Peptide, Ghrelin Antagonist, with Mesoporous Silicon Microparticles. *J. Controlled Release* **2009**, *137*, 166−170.

(8) Kilpeläinen, M.; Mönkäre, J.; Vlasova, M. A.; Riikonen, J.; Lehto, V.; Salonen, J.; Järvinen, K.; Herzig, K. Nanostructured Porous Silicon Microparticles Enable Sustained Peptide (Melanotan II) Delivery. *Eur. J. Pharm. Biopharm.* **2011**, *77*, 20−25.

(9) Tanaka, T.; Mangala, L. S.; Vivas-Mejia, P. E.; Nieves-Alicea, R.; Mann, A. P.; Mora, E.; Han, H.; Shahzad, M. M. K.; Liu, X.; Bhavane,

R.; Gu, J.; Fakhoury, J. R.; Chiappini, C.; Lu, C.; Matsuo, K.; Godin, B.; Stone, R. L.; Nick, A. M.; Lopez-Berestein, G.; Sood, A. K.; Ferrari, M. Sustained Small Interfering RNA Delivery by Mesoporous Silicon Particles. *Cancer Res.* **2010**, *70*, 3687−3696.

(10) Tasciotti, E.; Liu, X.; Bhavane, R.; Plant, K.; Leonard, A. D.; Price, B. K.; Cheng, M. M.; Decuzzi, P.; Tour, J. M.; Robertson, F.; Ferrari, M. Mesoporous Silicon Particles as a Multistage Delivery System for Imaging and Therapeutic Applications. *Nat. Nanotechnol.* **2008**, *3*, 151−157.

(11) Godin, B.; Gu, J.; Serda, R. E.; Bhavane, R.; Tasciotti, E.; Chiappini, C.; Liu, X.; Tanaka, T.; Decuzzi, P.; Ferrari, M. Tailoring the Degradation Kinetics of Mesoporous Silicon Structures Through PEGylation. *J. Biomed. Mater. Res., Part A* **2010**, *94A*, 1236−1243.

(12) Canham, L. T.; Reeves, C. L.; Newey, J. P.; Houlton, M. R.; Cox, T. I.; Buriak, J. M.; Stewart, M. P. Derivatized Mesoporous Silicon with Dramatically Improved Stability in Simulated Human Blood Plasma. *Adv. Mater.* **1999**, *11*, 1505−1507.

(13) Dobrovolskaia, M. A.; Aggarwal, P.; Hall, J. B.; McNeil, S. E. Preclinical Studies To Understand Nanoparticle Interaction with the Immune System and Its Potential Effects on Nanoparticle Biodistribution. *Mol. Pharmaceutics* **2008**, *5*, 487−495.

(14) Cedervall, T.; Lynch, I.; Lindman, S.; Berggård, T.; Thulin, E.; Nilsson, H.; Dawson, K. A.; Linse, S. Understanding the Nanoparticle−Protein Corona Using Methods to Quantify Exchange Rates and Affinities of Proteins for Nanoparticles. *Proc. Natl. Acad. Sci. U.S.A.* **2007**, *104*, 2050−2055.

(15) Walczyk, D.; Bombelli, F. B.; Monopoli, M. P.; Lynch, I.; Dawson, K. A. What the Cell "Sees" in Bionanoscience. *J. Am. Chem. Soc.* **2010**, *132*, 5761−5768.

(16) Aggarwal, P.; Hall, J. B.; McLeland, C. B.; Dobrovolskaia, M. A.; McNeil, S. E. Nanoparticle Interaction with Plasma Proteins as it Relates to Particle Biodistribution, Biocompatibility and Therapeutic Efficacy. *Adv. Drug Delivery Rev.* **2009**, *61*, 428−437.

(17) Gessner, A.; Waicz, R.; Lieske, A.; Paulke, B.; Mäder, K.; Müller, R. H. Nanoparticles with Decreasing Surface Hydrophobicities: Influence on Plasma Protein Adsorption. *Int. J. Pharm.* **2000**, *196*, 245−249.

(18) Gessner, A.; Lieske, A.; Paulke, B.; Müller, R. H. Functional Groups on Polystyrene Model Nanoparticles: Influence on Protein Adsorption. *J. Biomed. Mater. Res., Part A* **2003**, *65A*, 319−326.

(19) Tenzer, S.; Docter, D.; Rosfa, S.; Wlodarski, A.; Kuharev, J.; Rekik, A.; Knauer, S. K.; Bantz, C.; Nawroth, T.; Bier, C.; Sirirattanapan, J.; Mann, W.; Treuel, L.; Zellner, R.; Maskos, M.; Schild, H.; Stauber, R. H. Nanoparticle Size Is a Critical Physicochemical Determinant of the Human Blood Plasma Corona: A Comprehensive Quantitative Proteomic Analysis. *ACS Nano* **2011**, *5*, 7155−7167.

(20) Owens, D. E. III; Peppas, N. A. Opsonization, Biodistribution, and Pharmacokinetics of Polymeric Nanoparticles. *Int. J. Pharm.* **2006**, *307*, 93−102.

(21) Simberg, D.; Park, J.; Karmali, P. P.; Zhang, W.; Merkulov, S.; McCrae, K.; Bhatia, S. N.; Sailor, M.; Ruoslahti, E. Differential Proteomics Analysis of the Surface Heterogeneity of Dextran Iron Oxide Nanoparticles and the Implications for Their In Vivo Clearance. *Biomaterials* **2009**, *30*, 3926−3933.

(22) Ogawara, K.; Furumoto, K.; Nagayama, S.; Minato, K.; Higaki, K.; Kai, T.; Kimura, T. Pre-coating with Serum Albumin Reduces Receptor-Mediated Hepatic Disposition of Polystyrene Nanosphere: Implications for Rational Design of Nanoparticles. *J. Controlled Release* **2004**, *100*, 451−455.

(23) Tanaka, T.; Godin, B.; Bhavane, R.; Nieves-Alicea, R.; Gu, J.; Liu, X.; Chiappini, C.; Fakhoury, J. R.; Amra, S.; Ewing, A.; Li, Q.; Fidler, I. J.; Ferrari, M. In Vivo Evaluation of Safety of Nanoporous Silicon Carriers Following Single and Multiple Dose Intravenous Administrations in Mice. *Int. J. Pharm.* **2010**, *402*, 190−197.

(24) Serda, R. E.; Gu, J.; Bhavane, R. C.; Liu, X.; Chiappini, C.; Decuzzi, P.; Ferrari, M. The Association of Silicon Microparticles with Endothelial Cells in Drug Delivery to the Vasculature. *Biomaterials* **2009**, *30*, 2440−2448.

(25) Park, J.; Gu, L.; von Maltzahn, G.; Ruoslahti, E.; Bhatia, S. N.; Sailor, M. J. Biodegradable Luminescent Porous Silicon Nanoparticles for In Vivo Applications. *Nat. Mater.* **2009**, *8*, 331−336.

(26) Hakanpää, J.; Paananen, A.; Askolin, S.; Nakari-Setälä, T.; Parkkinen, T.; Penttilä, M.; Linder, M. B.; Rouvinen, J. Atomic Resolution Structure of the HFBII Hydrophobin, a Self-assembling Amphiphile. *J. Biol. Chem.* **2004**, *279*, 534−539.

(27) Linder, M. B. Hydrophobins: Proteins that Self-Assemble at Interfaces. *Curr. Opin. Colloid Interface Sci.* **2009**, *14*, 356−363.

(28) Haas Jimoh Akanbi, M.; Post, E.; Meter-Arkema, A.; Rink, R.; Robillard, G. T.; Wang, X.; Wösten, H. A. B.; Scholtmeijer, K. Use of Hydrophobins in Formulation of Water Insoluble Drugs for Oral Administration. *Colloids Surf., B* **2010**, *75*, 526−531.

(29) Valo, H. K.; Laaksonen, P. H.; Peltonen, L. J.; Linder, M. B.; Hirvonen, J. T.; Laaksonen, T. J. Multifunctional Hydrophobin: Toward Functional Coatings for Drug Nanoparticles. *ACS Nano* **2010**, *4*, 1750−1758.

(30) Varjonen, S.; Laaksonen, P.; Paananen, A.; Valo, H.; Hahl, H.; Laaksonen, T.; Linder, M. B. Self-Assembly of Cellulose Nanofibrils by Genetically Engineered Fusion Proteins. *Soft Matter* **2011**, *7*, 2402−2411.

(31) Valo, H.; Kovalainen, M.; Laaksonen, P.; Häkkinen, M.; Auriola, S.; Peltonen, L.; Linder, M.; Järvinen, K.; Hirvonen, J.; Laaksonen, T. Immobilization of Protein-Coated Drug Nanoparticles in Nanofibrillar Cellulose Matrices—Enhanced Stability and Release. *J. Controlled Release* **2011**, *156*, 390−397.

(32) Bimbo, L. M.; Mäkilä, E.; Raula, J.; Laaksonen, T.; Laaksonen, P.; Strommer, K.; Kauppinen, E. I.; Salonen, J.; Linder, M. B.; Hirvonen, J.; Santos, H. A. Functional Hydrophobin-Coating of Thermally Hydrocarbonized Porous Silicon Microparticles. *Biomaterials* **2011**, *32*, 9089−9099.

(33) Janssen, M. I.; van Leeuwen, M. B. M.; Scholtmeijer, K.; van Kooten, T. G.; Dijkhuizen, L.; Wösten, H. A. B. Coating with Genetic Engineered Hydrophobin Promotes Growth of Fibroblasts on a Hydrophobic Solid. *Biomaterials* **2002**, *23*, 4847−4854.

(34) Scholtmeijer, K.; Janssen, M. I.; Gerssen, B.; de Vocht, M. L.; van Leeuwen, B. M.; van Kooten, T. G.; Wosten, H. A. B.; Wessels, J. G. H. Surface Modifications Created by Using Engineered Hydrophobins. *Appl. Environ. Microbiol.* **2002**, *68*, 1367−1373.

(35) Aimanianda, V.; Bayry, J.; Bozza, S.; Kniemeyer, O.; Perruccio, K.; Elluru, S. R.; Clavaud, C.; Paris, S.; Brakhage, A. A.; Kaveri, S. V.; Romani, L.; Latge, J. Surface Hydrophobin Prevents Immune Recognition of Airborne Fungal Spores. *Nature* **2009**, *460*, 1117−1121.

(36) Bimbo, L. M.; Sarparanta, M.; Santos, H. A.; Airaksinen, A. J.; Mäkilä, E.; Laaksonen, T.; Peltonen, L.; Lehto, V.; Hirvonen, J.; Salonen, J. Biocompatibility of Thermally Hydrocarbonized Porous Silicon Nanoparticles and their Biodistribution in Rats. *ACS Nano* **2010**, *4*, 3023−3032.

(37) Salonen, J.; Björkqvist, M.; Laine, E.; Niinistö, L. Stabilization of Porous Silicon Surface by Thermal Decomposition of Acetylene. *Appl. Surf. Sci.* **2004**, *225*, 389−394.

(38) Sarparanta, M.; Mäkilä, E.; Heikkilä, T.; Salonen, J.; Kukk, E.; Lehto, V.; Santos, H. A.; Hirvonen, J.; Airaksinen, A. J. ^{18}F-Labeled Modified Porous Silicon Particles for Investigation of Drug Delivery Carrier Distribution in Vivo with Positron Emission Tomography. *Mol. Pharmaceutics* **2011**, *8*, 1799−1806.

(39) Bolton, A. E.; Hunter, W. M. The Labelling of Proteins to High Specific Radioactivities by Conjugation to a ^{125}I-Containing Acylating Agent. *Biochem. J.* **1973**, *133*, 529−538.

(40) Li, C.; Greenwood, T. R.; Bhujwalla, Z. M.; Glunde, K. Synthesis and Characterization of Glucosamine-Bound Near-Infrared Probes for Optical Imaging. *Org. Lett.* **2006**, *8*, 3623−3626.

(41) Cox, A. R.; Cagnol, F.; Russell, A. B.; Izzard, M. J. Surface Properties of Class II Hydrophobins from Trichoderma reesei and Influence on Bubble Stability. *Langmuir* **2007**, *23*, 7995−8002.

(42) Santos, H. A.; Riikonen, J.; Salonen, J.; Mäkilä, E.; Heikkilä, T.; Laaksonen, T.; Peltonen, L.; Lehto, V.; Hirvonen, J. In Vitro Cytotoxicity of Porous Silicon Microparticles: Effect of the Particle

Concentration, Surface Chemistry and Size. *Acta Biomater.* **2010**, *6*, 2721−2731.
(43) Choi, J.; Zhang, Q.; Reipa, V.; Wang, N. S.; Stratmeyer, M. E.; Hitchins, V. M.; Goering, P. L. Comparison of Cytotoxic and Inflammatory Responses of Photoluminescent Silicon Nanoparticles with Silicon Micron-Sized Particles in RAW 264.7 macrophages. *J. Appl. Toxicol.* **2009**, *29*, 52−60.
(44) Serda, R. E.; Blanco, E.; Mack, A.; Stafford, S. J.; Amra, S.; Li, Q.; van, d.V.; Tanaka, T.; Torchilin, V. P.; Wiktorowicz, J. E.; Ferrari, M. Proteomic Analysis of Serum Opsonins Impacting Biodistribution and Cellular Association of Porous Silicon Microparticles. *Mol. Imaging* **2011**, *10*, 43−55.
(45) Charkes, N. D.; Brookes, M.; Makler, P. T. Jr. Studies of Skeletal Tracer Kinetics: II. Evaluation of a Five-Compartment Model of [^{18}F]fluoride Kinetics in Rats. *J. Nucl. Med.* **1979**, *20*, 1150−1157.
(46) Vroman, L.; Adams, A.; Fischer, G.; Munoz, P. Interaction of High Molecular Weight Kininogen, Factor XII, and Fibrinogen in plasma at interfaces. *Blood* **1980**, *55*, 156−159.
(47) Göppert, T. M.; Müller, R. H. Adsorption Kinetics of Plasma Proteins on Solid Lipid Nanoparticles for Drug Targeting. *Int. J. Pharm.* **2005**, *302*, 172−186.
(48) Swanson, J. A.; Hoppe, A. D. The Coordination of Signaling During Fc Receptor-Mediated Phagocytosis. *J. Leukocyte Biol.* **2004**, *76*, 1093−1103.
(49) Moghimi, S. M.; Hunter, A. C.; Murray, J. C. Long-Circulating and Target-Specific Nanoparticles: Theory to Practice. *Pharmacol. Rev.* **2001**, *53*, 283−318.
(50) Dams, E. T. M.; Laverman, P.; Oyen, W. J. G.; Storm, G.; Scherphof, G. L.; van der Meer, J. W. M.; Corstens, F. H. M.; Boerman, O. C. Accelerated Blood Clearance and Altered Biodistribution of Repeated Injections of Sterically Stabilized Liposomes. *J. Pharmacol. Exp. Ther.* **2000**, *292*, 1071−1079.
(51) Yan, X.; Kuipers, F.; Havekes, L. M.; Havinga, R.; Dontje, B.; Poelstra, K.; Scherphof, G. L.; Kamps, J. A. A. M. The Role of Apolipoprotein E in the Elimination of Liposomes from Blood by Hepatocytes in the Mouse. *Biochem. Biophys. Res. Commun.* **2005**, *328*, 57−62.
(52) Bartl, M. M.; Luckenbach, T.; Bergner, O.; Ullrich, O.; Koch-Brandt, C. Multiple Receptors Mediate apoJ-Dependent Clearance of Cellular Debris into Nonprofessional Phagocytes. *Exp. Cell Res.* **2001**, *271*, 130−141.
(53) Soo Choi, H.; Liu, W.; Misra, P.; Tanaka, E.; Zimmer, J. P.; Itty Ipe, B.; Bawendi, M. G.; Frangioni, J. V. Renal Clearance of Quantum Dots. *Nat. Biotechnol.* **2007**, *25*, 1165−1170.